A High-order Finite Element Method for Electrical Impedance Tomography

S. Pursiainen and H. Hakula
Helsinki University of Technology, Finland

Abstract—Electrical impedance tomography (EIT) is a non-invasive imaging technique where a conductivity distribution in a domain is reconstructed from boundary voltage measurements. The voltage data are generated by injecting currents into the domain. This is an ill-conditioned non-linear inverse problem. Small measurement or forward modeling errors can lead to unbounded fluctuations in the reconstructions. A forward model describes the dependence of the noiseless voltage data on the conductivity distribution. The present work focuses on applying the high-order finite element method (p-FEM) for forward modeling. In the traditional version of the finite element method (h-FEM), the polynomial degree of the element shape functions is relatively low and the discretization error is reduced by increasing the number of elements. In the p-version, in contrast, the polynomial degree is increased and the mesh size is kept constant. In many applications of the finite element method the performance of the p-version is better than that of the h-version. In this work, it is proposed that the p-version provides more efficient tool for EIT forward modeling. Numerical results are presented.

1. Introduction

The electrical impedance tomography (EIT) problem is to reconstruct an unknown conductivity distribution σ in an object Ω from a set of noisy voltage measurements performed on the boundary $\partial\Omega$ This problem was first introduced in 1980 by Calderón [1]. At the present, EIT has numerous applications. These include detection of tumors from breast tissue [5], measuring brain function [8], imaging of fluid flows in process pipelines [10], and non-destructive testing of materials [13]. For a review on EIT, see Cheney *et al.*, [2].

In the present version of electrical impedance tomography, a current pattern $I = (I_1, I_2, \ldots, I_L)$ is injected into a two dimensional domain Ω through a set of contact electrodes e_1, e_2, ..., e_L placed on the boundary $\partial\Omega$. The injected currents induce a potential field u in the domain and a electrode voltages $U = (U_1, U_2, \ldots, U_L)$. The measurement data are gathered by injecting a set of linearly independent current patterns and measuring the corresponding electrode voltages. The conductivity distribution in Ω is to be reconstructed from these voltage measurements. This is a non-linear ill-conditioned inverse problem: small errors in the measurements or in the forward modeling can produce large errors in the reconstructions.

The focus of this paper is in efficient forward modeling. A forward model describes the dependence of the noiseless voltage data on the conductivity distribution. The complete electrode model by Somersalo et al., [9] and its simulations through the traditional finite element method (h-FEM) and the high-order finite element method (p-FEM) are considered. According to the complete electrode model, the potential distribution in the domain and the voltages on the electrodes can be determined by solving an elliptic boundary value problem. Finite element simulation of this forward model has been described by Vauhkonen [12]. In the h-version of FEM, the polynomial order p of the element shape functions is relatively low and the discretization error is reduced by decreasing the element size h. In the p-version, in contrast, the polynomial order is increased and the mesh size is kept constant. Processes where either the mesh is refined or the polynomial degree is increased are called $h-$ and p-extensions, respectively. Both extension processes increase the dimension of the finite element space which is denoted by N. Combinations of $h-$ and p-extensions are called hp-extensions (hp-FEM). Descriptions of $h-$, $p-$ and hp-versions of FEM are given e. g., in a book by Szabo and Babuska [11].

This work presents numerical results on performances of $h-$ and p-extensions in finite element simulation of the complete electrode model. The motivation for this study is that the solution of the complete electrode model equations can be very smooth in the interior part of Ω and that in finite element computations, it is typical that p-extensions are very efficient in problems with smooth solutions. For example, when the Poisson equation $\Delta u = f$ in a two-dimensional domain Ω with zero boundary conditions on $\partial\Omega$ has a smooth solution and uniform mesh refinement is used, the finite element solution u_h satisfies the inequality $\|u - u_h\|_{H^1(\Omega)} \leq Ch_p$, where h is the mesh size, p is the polynomial degree, C is some constant, and $H^1(\Omega)$ denotes the corresponding Sobolev space norm. Since in two dimensions the dimension of the finite element space N grows at the rate $O(p^2/h^2)$, one can deduce from the inequality, that as a function of N the error $\|u - u_h\|_{H^1(\Omega)}$ cannot converge

slower in p-extensions than in h-extensions. For detailed description on $h-$, $p-$ and hp-convergence, see Gui and Babuska [4].

2. Finite Element Simulation of the Complete Electrode Model

In the complete electrode model, the effective contact impedance between the electrode e_l and the boundary is characterized by the number $z_\ell > 0$. The electrode voltages U induced by the current pattern I can be found by solving the elliptic boundary value problem described by the equation

$$\nabla \cdot (\sigma \nabla u) = 0 \tag{1}$$

in the domain Ω, by the boundary conditions

$$\sigma \frac{\partial u}{\partial n}\Big|_{\partial\Omega \setminus \cup e_\ell} = 0, \quad \int_{e_\ell} \sigma \frac{\partial u}{\partial n}\, dS = I_\ell \quad \text{and} \quad \Big(u + z_\ell \sigma \frac{\partial u}{\partial n}\Big)\Big|_{e_\ell} = U_\ell, \qquad \ell = 1, 2, \ldots, L, \tag{2}$$

on $\partial\Omega$ and by Kirchoff's current and voltage laws $\sum_{\ell=1}^{L} I_\ell = 0$ and $\sum_{\ell=1}^{L} U_\ell = 0$. According to Somersalo *et al.*, [9], with certain assumptions made on the domain and on the conductivity distribution, there exists a unique pair $u \in H^1(\Omega)$ and $U \in \mathbb{R}^L$ that satisfies the weak formulation of this problem. The finite element solution of these equations is the pair

$$u_{FE} = \sum_{i=1}^{N} \alpha_i \varphi_i \quad \text{and} \quad U_{FE} = \sum_{i=1}^{L-1} \beta_i (e_1 - e_{i+1}), \tag{3}$$

where $\varphi_1, \varphi_2, \ldots, \varphi_N$ are the shape functions of the finite element space and $e_1, e_2, \ldots, e_L$ are the standard basis vectors of $\mathbb{R}^L$. The coefficients $\alpha_1, \alpha_2, \ldots, \alpha_N$ and $\beta_1, \beta_2, \ldots, \beta_N$ can be found by solving the linear system of equations $Ax = b$. The entries of the vectors x and b are given by $x_i = \alpha_i$ and $b_i = 0$ if $i \le N$, otherwise $x_i = \beta_{i-N}$ and $b_i = (e_1 - e_{i+1-N})^T I$. The system matrix entries are given by

$$A_{i,j} = \begin{cases} \int_\Omega \sigma \nabla \varphi_i \cdot \nabla \varphi_j \, dxdy + \sum_{\ell=1}^{L} \frac{1}{z_\ell} \int_{e_\ell} \varphi_i \varphi_j \, ds, & \text{if} \quad 1 \le N \quad \text{and} \quad j \le N, \\ -\frac{1}{z_1} \int_{e_1} \varphi_i \, ds + \frac{1}{z_{j+1-N}} \int_{e_{j+1-N}} \varphi_i \, ds, & \text{if} \quad i \le N \quad \text{and} \quad j > N, \\ \frac{1}{z_1} \int_{e_1} ds + \frac{\delta_{i,j}}{z_{j+1-N}} \int_{e_{j+1-N}} ds, & \text{if} \quad i > N \quad \text{and} \quad j > N. \end{cases} \tag{4}$$

where $\delta_{i,j}$ is the Kronecker delta.

3. Hierarchic Shape Functions for p-extensions

In the standard p-version of the finite element method, the shape functions used in p-extensions are hierarchic. In this context, the term hierarchic means that the set of shape functions of polynomial order p is in the set of shape functions of order $p+1$, and the number of shape functions which do not vanish at the vertices and the sides of the elements is minimal. Hierarchic shape functions are constructed by using Legendre polynomials

$$P_n(x) = \frac{1}{2^n n!} \frac{d^n}{dx^n} (x^2 - 1)^n, \qquad n = 0, 1, \ldots \quad . \tag{5}$$

Due to the orthogonality properties of these polynomials, hierarchic shape functions are well-suited for computer implementation and have very favorable properties from the point of view of numerical stability [11].

In the one-dimensional case, the standard element is the interval $[-1, 1]$. For this element, the one-dimensional hierarchic shape functions of polynomial order p are defined as

$$N_1(\xi) = \frac{1-\xi}{2}, \quad N_2(\xi) = \frac{1+\xi}{2}, \quad N_n(\xi) = \phi_{n-1}(\xi), \qquad n = 3, 4, \ldots, p+1, \tag{6}$$

where ϕ_n is defined as $\phi_n(\xi) = \sqrt{n - 1/2} \int_{-1}^{\xi} P_{n-1}(\xi)\, dt$. These are organized to two categories. The first one is formed by the polynomials N_1 and N_2, that are called the nodal shape functions, the external shape functions, or the vertex modes. The higher order polynomials N_3, N_4, ..., N_{p+1} form the second category. These vanish at the endpoints of the interval $[-1, 1]$ and they are called the bubble functions, the internal shape functions, or the internal modes.

The two-dimensional quadrilateral standard element is the square $[-1,1]\times[-1,1]$. The corresponding two-dimensional hierarchical shape functions of polynomial order p are products of one-dimensional shape functions.

$$\begin{aligned} N_{n,m}(\xi,\eta) &= \frac{1}{4}(1+(-1)^n\xi)(1+(-1)^m\eta), && n=1,2, && m=1,2, \\ N^{(0)}_{n,m}(\xi,\eta) &= \phi_n(\xi)\phi_m(\eta), && n=2,3,\ldots,p, && m=2,3,\ldots,p, \\ N^{(1)}_{n}(\xi,\eta) &= \frac{1}{2}(1-\eta)\phi_n(\xi), && n=2,3,\ldots,p, \\ N^{(2)}_{n}(\xi,\eta) &= \frac{1}{2}(1-\xi)\phi_n(\eta), && n=2,3,\ldots,p. \end{aligned} \tag{7}$$

These are organized to three categories: vertex modes $N_{n,m}$, internal modes $N^{(0)}_{n,m}$, and side modes $N^{(1)}_n$, $N^{(2)}_n$. In this work, only quadrilateral elements are used. Construction of hierarchical shape functions for triangular elements has been described e. g., in [11].

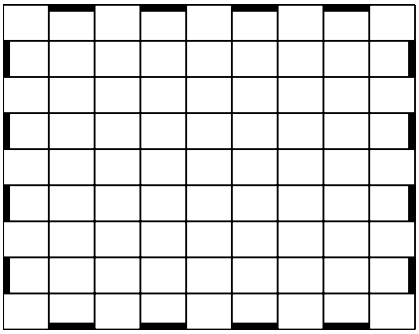

Figure 1: The square shaped domain, the locations of the 16 electrodes, and the coarsest mesh ($h_0 = 1/9$) used in the computations.

4. Numerical Experiments

Numerical experiments were performed concerning performances of h- and p-extensions in FEM simulation of the complete electrode model. In these computations, the domain Ω was the unit square $[0,1]\times[0,1]$ and the conductivity distribution σ in Ω was identically one. Sixteen electrodes with equal contact impedances $z_1 = z_2 = \ldots = z_\ell = 1$ were placed evenly on the boundary (Fig. 1). All the contact impedances were assumed to be equal to one. The generated voltage data constisted of $L-1$ electrode voltage vectors $U^{(1)}, U^{(2)}, \ldots, U^{(L-1)}$ induced by pair drive [7] current patterns $I^{(1)}, I^{(2)}, \ldots, I^{(L-1)}$ such that $I^{(k)}_k = 1$ and $I^{(k)}_{k+1} = -1$ and all other entries are zero. In each of these current patterns, the two current injecting electrodes were located next to each other. The finite element method was used both in data generation and simulation. Each finite element mesh used in these computations consisted of equal-sized square shaped elements as illustrated in Fig. 1. In data simulation, bilinear and hierarchic shape functions were used in h- and p-extensions, respectively. One h-extension process and three p-extension processes were executed (Table 1). In these processes, elements of sizes $h = h_0, 2^{-1}h_0, \ldots, 2^{-7}h_0$ with $h_0 = 1/9$ and polynomial orders $p = 1,2,\ldots,8$ were employed. The growth of the dimension of the finite element space is reported in Table 1. In data generation, the size and the polynomial order of the elements were $h = 2^{-3}h_0$ and $p = 8$. A vector containing all the generated data is denoted by $\mathbf{U}_{EX}$ and a vector containing the simulated electrode voltages is denoted by $\mathbf{U}_{FE}$. Accuracy of the simulation is measured in ℓ^2-norm by the relative error

$$\mathrm{RE} = ||\mathbf{U}_{EX} - \mathbf{U}_{FE}||_2 / ||\mathbf{U}_{EX}||_2. \tag{8}$$

5. Results and Discussion

Figure 2 illustrates the convergence of the relative error (8) in the h- and p-extension processes. The relative error is plotted against the dimension of the finite element space on $\log_{10}$-$\log_{10}$ scale. The results show that p-convergence rate is faster than the rate of h-convergence.

In finite element computations, p-extensions are often motivated by the fact that the solution is smooth whereas h-extensions are favorable in the case of non-smooth solutions [11]. According to Evans [3], the interior

Table 1: The executed h- and p-extension processes: h- and p-values and finite element space dimensions. In data generation, the size and the polynomial order of the elements were $h = 2^{-3}h_0$ and $p = 8$ (down right corner).

index	type	h-values	p-values	finite element space dimensions							
(a)	h	$h_0, 2^{-1}h_0, \ldots, 2^{-7}h_0$	1	100	361	784	1369	2116	3025	4096	5329
(b)	p	h_0	$1, 2, \ldots, 8$	100	280	460	721	1063	1486	1990	2575
(c)	p	$2^{-1}h_0$	$1, 2, \ldots, 8$	361	1045	1729	2737	4069	5725	7705	10009
(d)	p	$2^{-3}h_0$	$1, 2, \ldots, 7$	1369	4033	6697	10657	15913	22465	30313	—

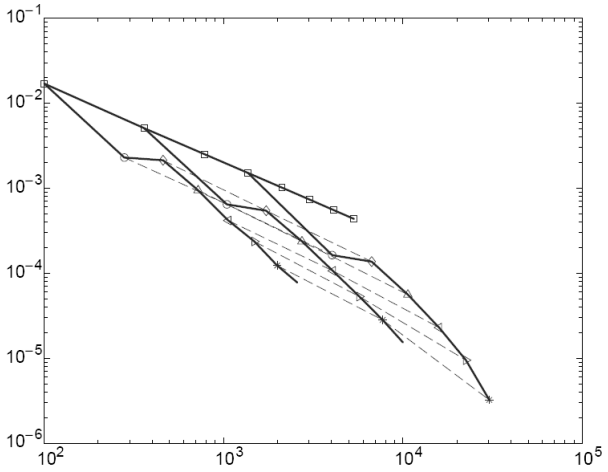

Figure 2: The relative error (8) in the executed $h-$ and p-extension processes (a), (b), (c) and (d) plotted against the dimension of the finite element space on $\log_{10}$-$\log_{10}$ scale. The straight line represents the h-extension process (a). The three curved lines from left to right represent the p-extension processes (b), (c) and (d) respectively. The dashed lines show the h-convergence rate in the cases where $p = 2$, 3, 4, 5, 6 or 7.

potential distribution $u \in H^1(\Omega)$ determined by the complete electrode model is smooth provided that the conductivity distribution is smooth. However, it is important to point out that the potential distribution is not smooth in the vicinity of the boundary, since according to the boundary conditions (2) the normal derivative $\partial u/\partial n$ is discontinuous on $\partial\Omega$. Consequently, it is possible that near the boundary the performance of h-extensions can be better than that of p-extensions. It is also important to note that electrical impedance tomography involves a variety of applications, e. g., detection of tumors, where the conductivity is a non-smooth or a discontinuous function. A local discontinuity in the conductivity distribution, e. g., a tumor, causes local non-smoothness of the interior potential distribution in the vicinity of the discontinuity [3]. This means that the structure of the conductivity can affect the performance of h- and p-extensions in different parts of the domain. In future work it would be interesting to explore performances of different hp-extension processes with different conductivity distributions. For example, whether *a priori* information about the conductivity distribution can be used when designing hp-extensions could be an issue in electrical impedance tomography.

From the computational point of view, one important difference in h- and p-extensions is that in p-extensions a lot more computational effort is spent on numerical integration when constructing the system matrix (4) due to the high polynomial order of the shape functions. Electrical impedance tomography involves reconstruction methods, e. g., Markov chain Monte Carlo sampling [6], where efficient forward modeling in terms of computation time is essential, because the forward model equations have to be solved numerous times during the reconstruction process. Another interesting future consideration would be whether there are computationally tractable ways to obtain system matrices needed in EIT reconstruction, e. g., whether *a priori* knowledge about the conductivity distribution can be used when constructing a system matrix.

6. Conclusion

In this work, the p-version of the finite element method was applied to simulation of the complete electrode model. The motivation for this study was that the solution of the complete electrode model equations can be smooth in the interior domain and that it is typical that the p-version is very efficient in problems with smooth solutions. It was shown numerically by using the unit square that the performance of the p-version is better than that of the h-version when uniform mesh refinement is used. Since the solution of the complete electrode model equations is non-smooth in the vicinity of the boundary, an important topic for the future work is to explore the performance of the hp-version of FEM. From the computational point of view, one characteristic difference in h- and p-versions of FEM is that in p-version a lot more computational effort is spent on construction of a system matrix. Another important future consideration is to find computationally tractable ways to obtain system matrices needed in EIT reconstruction. It is also an important issue whether *a priori* knowledge about the conductivity distribution can be used when designing a p-FEM implementation to be used in EIT reconstruction.

Acknowledgment

This work was supported by the Academy of Finland.

REFERENCES

1. Calderon, A. P., "On an inverse boundary value problem," *Seminar on Numerical Analysis and its Applications to Continuum Physics*, Soc. Brasil. Mat., Rio de Janeiro, 1980.
2. Cheney, M., D. Isaacson, and J. C. Newell, "Electrical impedance tomography," *SIAM Review*, Vol. 41, 85–101, 1999.
3. Evans, L. C., *Partial differential equations*, American Mathematical Society, Rhode Island, 308–316 1998.
4. Gui, W. and I. Babuska, "The h-,p- and hp-versions of the finite elemen method in one dimension. Part I: the error analysis of the p-version. Part II: the error analysis of the h- and hp-versions. Part III: the adaptive hp-version.," *Numerische Mathematik*, Vol. 49, 577–683, 1986.
5. Hartov, A., N. K. Soni, and K. D. Paulsen, "Variation in breast EIT measurements due to menstrual cycle," *Physiological Measurement*, Vol. 25, 295–299, 2004.
6. Kaipio, J. P., V. Kolehmainen, E. Somersalo, and M. Vauhkonen, "Statistical inversion and monte carlo sampling methods in electrical impedance tomography," *Inverse Problems*, Vol. 16, 1487–1522, 2000.
7. Lionheart, W. R. B., J. Kaipio, and C. N. McLeod, "Generalized optimal current patterns and electrical safety in EIT," *Physiol. Meas.*, Vol. 22, 85–90, 2001.
8. Polydorides, N., W. R. B. Lionheard, and H. McCann, "Krylov subspace iterative techniques: on the detection of brain activity with electrical impedance tomography," *IEEE Transactions on Medical Imaging*, Vol. 21, 596–603, 2002.
9. Somersalo, E., M. Cheney, and D. Isaacson, "Existence and uniqueness for electrode models for electric current computed tomography," *SIAM J. Appl. Math.*, Vol. 52, 1023–1040, 1992.
10. Stanley, S. J., R. Mann, and K. Primrose, "Tomographic imaging of fluid mixing in 3-d for single-feed semi-batch operation of a stirred vessel," *Chemical Engineering Research and Design*, Vol. 80, 903–909, 2002.
11. Szabo, B. and I. Babuska, *Finite Element Analysis*, John Wiley & Sons, New York, 1991.
12. Vauhkonen, M., *Electrical Impedance Tomography and Prior Information*, PhD Thesis, University of Kuopio, Kuopio, 1997.
13. Vilhunen, T., L. M. Heikkinen, T. Savolainen, P. J. Vauhkonen, R. Lappalainen, J. P. Kaipio, and M. Vauhkonen, "Detection of faults in resistive coatings with an impedance-tomography-related approach," *Measurement Science and Technology*, Vol. 13, 865–872, 2002.